

Significant noise improvement in a Kinetic Inductance Phonon-Mediated detector by use of a wideband parametric amplifier

K. Ramanathan,^{1,2,*} O. Wen,^{1,†} T. Aralis,³ R. Basu Thakur,⁴ B. Bumble,⁴ Y.-Y. Chang,⁵ P. K. Day,⁴ B. H. Eom,⁴ H. G. Leduc,⁴ B. J. Sandoval,¹ R. Stephenson,¹ and S. R. Golwala¹

¹*Department of Physics, California Institute of Technology, Pasadena, CA 91125, USA*

²*Department of Physics, Washington University in St. Louis, St. Louis, MO 63130, USA*

³*SLAC National Accelerator Laboratory, 2575 Sand Hill Rd, Menlo Park, CA 94025, USA*

⁴*Jet Propulsion Laboratory, California Institute of Technology, Pasadena, CA 91109, USA*

⁵*Department of Physics, University of California, Berkeley, CA 94720, USA*

(Dated: February 9, 2024)

Microwave Kinetic Inductance Detectors (MKIDs) have been demonstrated as capable phonon sensors when coupled to crystalline substrates, and have been proposed as detectors for next-generation rare-event searches such as for the direct detection of dark matter. These Kinetic Inductance Phonon-Mediated (KIPM) detector designs, favoring large superconducting absorber volumes and high readout powers, are oftentimes limited in their sensitivity by low temperature amplifier noise introduced in the signal readout chain. We report here an effort to couple a wideband Kinetic Inductance Traveling Wave Parametric Amplifier (KI-TWPA), operated near the Standard Quantum Limit of minimal added amplifier noise, to sensors spanning a 70 MHz bandwidth at 3.5 GHz. This results in a $\sim 5\times$ improvement in the inferred detector energy resolution in the best sensor and highlights the potential of constructing $O(100)$ meV resolving phonon-mediated particle detectors. We detail limitations introduced by lossy passive components, degraded RF responsivity, and microphysical noise sources like two-level systems (TLS), in achieving ultimate quantum-limited system noise levels.

I. INTRODUCTION AND MOTIVATION

Microwave Kinetic Inductance Detectors (MKIDs) are thin film superconducting LC microresonators that originated as photon sensors [1]. The resonator surface impedance contains a reactive component due to Cooper-pair inertia, termed the *kinetic inductance*. If an MKID absorbs energy from the environment that breaks Cooper-pairs (creating *quasiparticles*), the resultant change in kinetic inductance modulates the complex transmission S_{21} of a microwave frequency tone. This modulation can be interpreted as a shift of the resonant frequency ν_r and the internal quality factor Q_i of the resonator. Aided by the high quality factors achievable by superconducting devices ($Q_i > 10^6$ [2]), hundreds to thousands of narrow linewidth MKIDs of $\nu_r = O(\text{GHz})$ can be chained on a single RF feedline with $O(\text{MHz})$ spacing [3], providing for straightforward room temperature readout and operation. MKIDs have been used for numerous astrophysical applications ranging from sub-millimeter wavelength telescopes to optical exoplanet observatories [4].

The past decade has also seen the development of lumped-element¹ MKIDs [5] for use as Kinetic Inductance Phonon-Mediated detectors (KIPMs). In this concept, incident particles on a crystalline substrate (like silicon) create propagating lattice vibrations (*athermal phonons*) that couple to the MKID sensors patterned on the substrate's surfaces. With large gram to kilogram mass targets, these devices can be used as particle detectors for rare-event searches. For example, this phonon-mediated scheme has been demonstrated for x-ray detection

[6], for neutrinoless double-beta decay searches [7], and as future dark matter detectors [8, 9].

The effectiveness of KIPM detectors for particle physics applications hinges on their ability to reconstruct energies E with the smallest possible baseline energy resolution σ_E . From the derived expressions in Refs. [6, 10] we expect the energy resolution to scale as,

$$\sigma_E \propto \sqrt{T_{\text{sys}}} \quad (1)$$

in the case of a white noise *amplifier-limited* readout with overall system noise temperature T_{sys} . Two level system (TLS) noise, commonly arising from surface oxides, is another important source of noise in MKIDs and is expected to be subdominant in designs with large feature sizes of the capacitor [11]. Recent KIPM detector results have inferred a 5 eV energy resolution for an amplifier-limited detector and a 20 eV energy resolution for a TLS-limited detector [9]. At cryogenic millikelvin temperatures where temperature effects are non-linear [12], noise can be better expressed as linearized *noise quanta* via $N = (1/2)\coth(h\nu/2k_B T)$ [13], with units of photon per second per Hz of bandwidth. In this Letter, we demonstrate a strategy to minimize N_{sys} across a wide 70 MHz band, and compare it to the Standard Quantum Limit (SQL) of $N = 1^2$, the quantum mechanical lower bound of any experiment using signal amplification³ [13, 16].

With their large gain ($G > 30$ dB) and complementary wide bandwidth, high electron mobility transistor (HEMT) amplifiers are the dominant amplification technology used by

* karthikr@caltech.edu

† owwen@caltech.edu

¹ Rather than distributed inductive and capacitive elements.

² A combination of zero point vacuum fluctuations and amplifier added noise. The SQL technically refers to the amplifier added 1/2 photon contribution, but here we consider the effective noise bound for an actual experiment.

³ Though techniques like "squeezing" may help surmount this bound [14, 15]

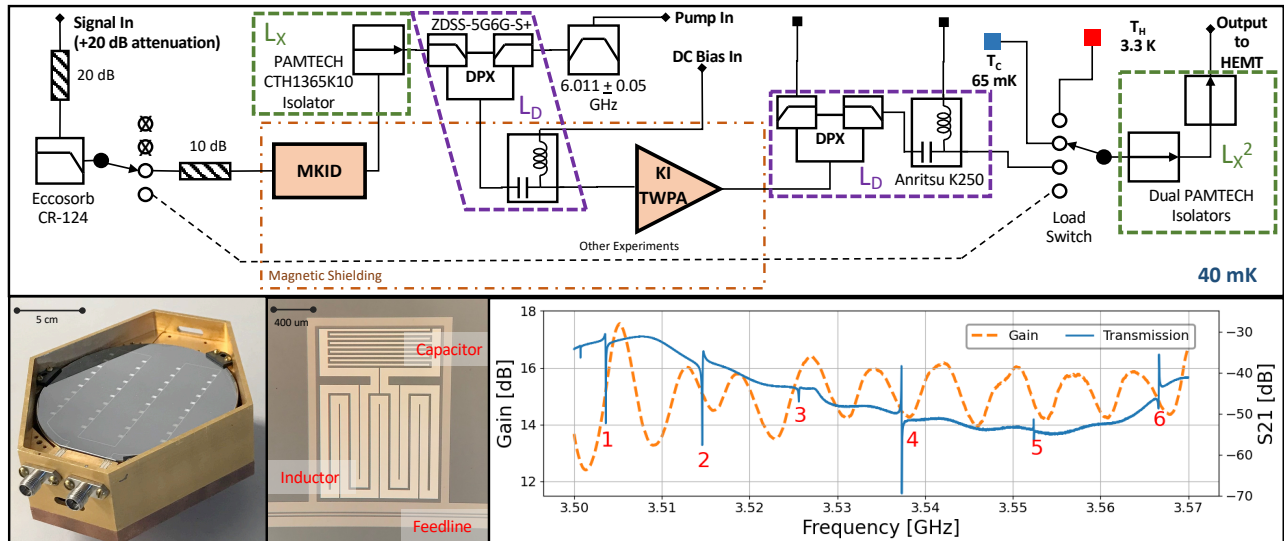


FIG. 1: *Top*: Schematic of cold stage of experiment, with labeled components. Thick dashed lines indicate groupings labeled by their losses L_D , L_X , and L_X^2 of passive components referred to in Sec. III. *Bottom Left*: Picture of 40 MKID array used in experiment showing the gold plated copper device holder, with cirlex clamped silicon substrate, along with a micrograph of a single MKID, outlining the constituent circuit features. *Bottom Right*: Transmission S_{21} of the MKID array, showing the numbered Al resonators used in the analysis (leftmost resonance feature is a Nb resonator). Overlaid is the smoothed gain, G_{pa} , of KI-TWPA in detector band, as measured between KI-TWPA on and off conditions.

present MKID experiments for simultaneous readout of all sensors. However, with nominal noise temperatures of > 3.5 K at C-band frequencies (4–8 GHz), these devices add $O(10)$ quanta of noise to any measurement. As Eq. 1 would dictate then, a theoretical improvement of $> 4\times$ the resolution would be achievable through quantum limited operation.

Kinetic Inductance Traveling Wave Parametric Amplifiers (KI-TWPAs) are a class of quantum limited amplifiers which also exploit principles of kinetic inductance, but for exactly such low-noise amplification [17]. They have been demonstrated to reach the SQL limit of added amplifier noise [18] and have previously been integrated with optical MKIDs [19]. In this paper we demonstrate the noise improvement achievable in a KIPM detector that is coupled to a KI-TWPA that offers broadband gain and low noise performance for future rare-event search experiments.

II. SETUP AND MEASUREMENT

The cold stage components of the experiment are laid out in the schematic of Fig. 1 Top. The MKID array used in this experiment was designed and fabricated based on parameters and principles found in Ref. [20]. It has 40 sensors, 16 made of 30 nm thick Aluminum and 24 made of 30 nm Niobium, coupled to a 300 nm thick Nb feedline and deposited on a 3 inch wafer as seen in Fig. 1 Bottom Left. The sensors span ν_r from approx. 3.0 GHz to 3.6 GHz and have overall/loaded quality factors Q_r ($= 1/Q_i + 1/Q_c$, where Q_c is the coupling quality factor) between 10^3 – 10^5 , with the variation in the latter likely due to the large differences in S_{21}

transmission across the operating band [8], as seen in Fig. 1 Bottom Right. For this exercise we operated the KIPM detector in a dilution refrigerator at $T_0 = 40 \pm 1$ mK and collected data from 6 Al MKIDs in the 3.5–3.6 GHz range, using individual readout tones generated by a room-temperature signal generator with cold stage attenuation and filtering to reduce input noise. Aluminum films are of interest as phonon sensors due to their phonon collection efficiency, their low gap energy ($\Delta \sim 200$ μ eV), and their long quasiparticle lifetimes [6, 21]. These specific MKID sensors were chosen because they had the highest transmission amongst all candidates. The array was connected to a NbTiN KI-TWPA operated in 3-wave mixing mode (operational details found in Ref. [18]), with associated passive diplexers and bias tees for introducing and dumping the 6.11 GHz pump tone and DC bias current I_{DC} required for the KI-TWPA’s operation. In addition, the setup used 3 identical isolators to reduce harmful reflections. The output was fed to a cold switch, with other throws linked to a “hot” (3.38 ± 0.05 K) and “cold” (65 ± 1 mK) load (Johnson noise source) for calibration purposes. The output was further amplified by a HEMT (LNF-LNC03.14A with a vendor specified gain of 39 dB and noise temperature of 3.6 K at 3.5 GHz) and a 27 dB room temperature amplifier. Signal processing was done using either a homodyne setup (IQ mixer fed to a PCI-E DAQ card) or direct connection to a spectrum analyzer (SA) / vector network analyzer (VNA) for calibration.

Three separate measurements were performed, allowing determination of the KI-TWPA gain, the system noise, and individual resonator noise. The KI-TWPA gain was measured using the VNA and measuring the difference in transmission with the DC bias and pump tone turned on/off. The measured

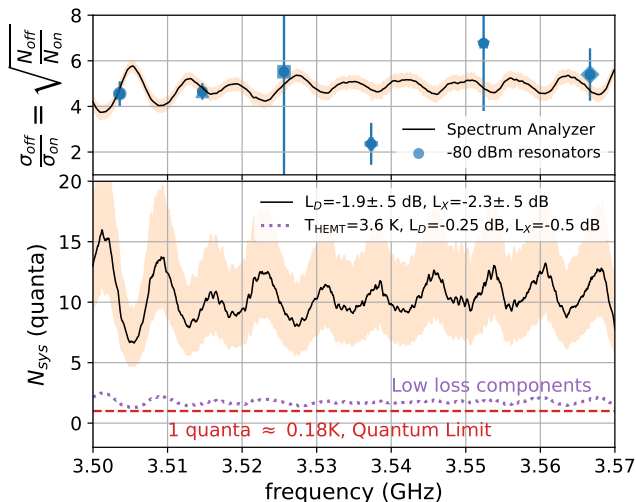


FIG. 2: *Top*: Resolution improvement as observed from both the spectrum analyzer and individual lowest power resonator data, with $\pm 1\sigma$ power measurement uncertainty shown by the shaded band. *Bottom*: Total system noise quanta with the KI-TWPA on, as referred to the input of the first diplexer. The shaded region reflects systematics on the passive component attenuations sandwiching the KI-TWPA (see Fig. 1). Using datasheet and prior measurement values results in the solid (black) line, indicating about 10 quanta of added noise with a minima around 7 quanta. The dotted purple line shows near SQL performance is achievable with better cold circuitry.

~ 15 dB gain profile (G_{pa}) of the KI-TWPA is shown in Fig. 1 Bottom Right. The relatively low gain is attributed to a smaller than expected critical current parameter for the specific device, not allowing it to be driven with a larger pump & bias. The observed ripples, of $O(\text{MHz})$ periodicity, are likely sourced from an impedance mismatch between the parametric amplifier and other circuitry, as described in Ref. [18].

The calibration of the added noise and system noise temperature was done using the aforementioned cold-switch setup with the output signal processed by a real-time spectrum analyzer. 4 power data sets were collected in this configuration: a 300 K terminated input with the KI-TWPA on (P_{on}) and off (P_{off}), along with the hot load (P_{H}) and cold load (P_{C}) measurements.

The final measurement used signal generator tones to collect IQ timestreams for each of the 6 resonators. For each resonator we recorded 10 s long timestreams at their respective ν_r , along with 0.5 s timestreams at 12 logarithmically spaced frequency intervals around $\pm 5\nu_r/Q_r$ including two far off resonance datasets at $\nu_r \pm 20\nu_r/Q_r$. These measurements were repeated at three powers $P_g = [-80, -68, -56]$ dBm (at device input) as well as for the KI-TWPA on and off conditions. All outputs were recorded at a sampling rate of 700 kS/s per quadrature and further digitally decimated by a factor of $10\times$.

III. SYSTEM NOISE CALIBRATION

With the gain measurement in hand we computed the resolution improvement in two independent ways, either using the spectrum analyzer or the individual resonator timestream datasets described above. For the former, we performed a standard Y-factor analysis (with linearized quantities as previously discussed) and refer to the groupings of passive elements from Fig. 1 Top (see thick dashed purple and green lines), generally following the prescriptions of Refs. [18, 19]. Under the condition that the HEMT dominates everything downstream of it the effective noise temperature of the isolator and HEMT package at the switch is,

$$T_{\text{switch}}^{\text{HEMT}}(\nu_r) \approx \frac{T_{\text{H}} - Y T_{\text{C}}}{(Y - 1)} = [9.5, 11.5] \pm 0.6 \text{ K}, \quad Y = P_{\text{H}}/P_{\text{C}} \quad (2)$$

which indicates that the HEMT noise, nominally 3.6 K, is worsened by the presence of the isolators.

Next, because the environment at the switch is fully characterized via the thermal power measurements, we obtained linear coefficients m and y_0 relating $(T_{\text{H}}, P_{\text{H}})$ and $(T_{\text{C}}, P_{\text{C}})$. We then computed the overall system noise at the input to the first isolator with the KI-TWPA either on or off as,

$$N_{\text{sys}}^{\text{on/off}} \approx \left(T_{\text{switch}}^{\text{HEMT}} + \frac{P_{\text{on/off}} - y_0}{m} \right) \left(\frac{L_D^2 L_X}{G_{\text{pa}}^{\text{on/off}}} \right) \left(\frac{k_B}{h\nu} \right) \quad (3)$$

Note that this calculation is the system noise as it pertains to the entire experiment — exactly the configuration when performing a rare-event search — and not just the added contribution from an SQL amplifier. We plot the expected resolution improvement as the root ratio of the on/off conditions of Eq. 3, as seen by the solid line in Fig. 2 Top, indicating an approximately $5\times$ improvement in energy resolution. The 1σ uncertainty band expressed there arises from variations within the power measurements affecting Y and $P_{\text{on/off}}$. The resonator points will be discussed in Sec. IV.

From datasheets and prior measurements we estimated the diplexer + bias-tee attenuation as $L_D = -1.9$ dB and the isolator $L_X = -2.2$ dB [22], leading to the system noise curve in Fig. 2 Bottom (along with systematic uncertainties), averaging $N_{\text{sys}} \approx 10$. A 4 K HEMT only measurement is expected to have $N_{\text{sys}} \approx 25$, which only suggests a $1.6\times$ resolution improvement for a rare-event search experiment when compared to our measurement. We resolve this tension by showing the effect of the lossy passive components on the result. In particular, while the post-switch multi-isolator attenuation L_X^2 is nominally factored out due to the switch location and our Eq. 2 prescription, we confirm its effect by fixing $T_{\text{HEMT}} = 3.6$ K and selecting feasibly low values for L_D and L_X , leading to the purple dotted line close to the SQL. Overall this suggests that further improvements will come both from refined operation of the KI-TWPA with higher gain ($G_{\text{pa}} \gtrsim 30$ dB [18]) and in carefully selecting for far less lossy passive components.

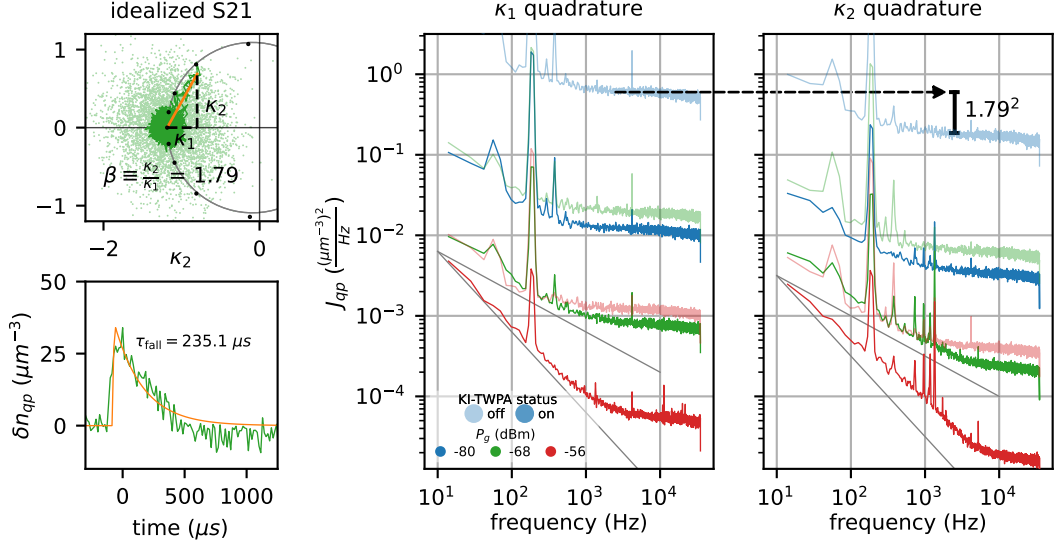


FIG. 3: *Top Left*: The idealized S_{21} timestream of KID 5 at -68 dBm, showing KI-TWPA on (off) data points in solid (faded), overlain on the unit normalized resonance circle (grey) with parameters derived from the fits to the VNA scan. The black points are the means of the IQ timestreams with the KI-TWPA on, measured at logarithmically spaced frequencies around ν_r and converted into idealized S_{21} . The green deviation is an observed pulse, and the orange line represents the expected pulse direction as given by Mattis-Bardeen theory. *Bottom Left*: Extracted change in quasiparticle density from the same pulse, with overlain single pole exponential fit. *Center, Right*: J_{qp} for KID 5 at various powers and with the KI-TWPA on and off, to illustrate the improvement in the noise with the KI-TWPA. f^{-1} and $f^{-0.5}$ have been drawn to guide the eye.

IV. RESONATOR NOISE CALIBRATION

The VNA data of each resonance was fit to the following form from Ref. [23]:

$$S_{21}(\nu) = a \cdot e^{2\pi i \nu \tau} \left(1 - \frac{Q_r |\hat{Q}_c|^{-1} e^{j\phi}}{1 + 2iQ_r x} \right) \quad (4)$$

for complex coupling quality factor \hat{Q}_c ⁴ parameterized in terms of its inverse magnitude and phase ϕ , complex off-resonance transmission a , cable delay τ , and resonant frequency detuning $x = (\nu - \nu_r)/\nu_r$.

The raw IQ data were converted into an idealized form by using the VNA fit parameters and the logarithmically spaced IQ timestreams shown in Fig. 3 Top Left. An example of the on-resonance idealized S_{21} data is displayed with the KI-TWPA both on and off. The improvement in readout noise can be seen directly as a decrease in the scatter of the noise points. At low readout powers, the conversion to the idealized S_{21} has an uncertainty that is dominated by the size estimation of the resonance circle in the IQ plane, and it is this uncertainty that is propagated into the error bars seen in Fig. 2 Top. Next, deviations about the mean idealized S_{21} were computed as a function of time t and cast as $\delta S_{21}(t)$. The timestreams were

converted into a *quasiparticle basis* (κ_1, κ_2) using the relation,

$$\delta S_{21}(t) = \alpha \frac{Q_r^2}{Q_c} (\kappa_1 + i\kappa_2) \delta n_{qp}(t), \quad (5)$$

where α is the kinetic inductance fraction of the film and $\kappa_{1,2}(T_0, \nu_r, \Delta)$ are derived from *Mattis-Bardeen* theory [24] and represent the film conductivity response to changing quasiparticle density. For small perturbations in the density, these orthogonal deviations can be used to identify δn_{qp} .

To obtain α and Δ , the temperature T was swept up to 350 mK, and $\nu_r(T)$ and $Q_r(T)$ were measured for each resonator. In general, either quadrature may be used to extract α and Δ , but only $\nu_r(T)$ was used in this analysis. $Q_r(T)$ showed evidence of non-thermal sources of dissipation, such as idealized resonance circles that encircle 0 (an example of which is in Fig. 3 Top Left), and consequent deviations from Mattis-Bardeen expectations, which prevented reliable extraction of α and Δ in the κ_1 quadrature.

The relative responsivities of the κ_1 and κ_2 quadratures can be expressed quantitatively as $\beta \equiv \kappa_2/\kappa_1$ and can be measured using the temperature sweeps as described previously or using the pulse shape of the S_{21} trajectory when incident energy is received by a particular MKID. There is also a theoretical expectation for β as given by $\kappa_{1,2}(T_0, \nu_r, \Delta)$. In Fig. 3 Top Left, the pulse shape of an *in situ* observed particle event displays good agreement with the theoretical response of the MKID. This agreement was not seen for all of the observed particle events in the various timestreams, of which there were only a handful, likely due to non-thermal sources of dissipation

⁴ \hat{Q}_c is now complex to account for impedance mismatches along the feedline.

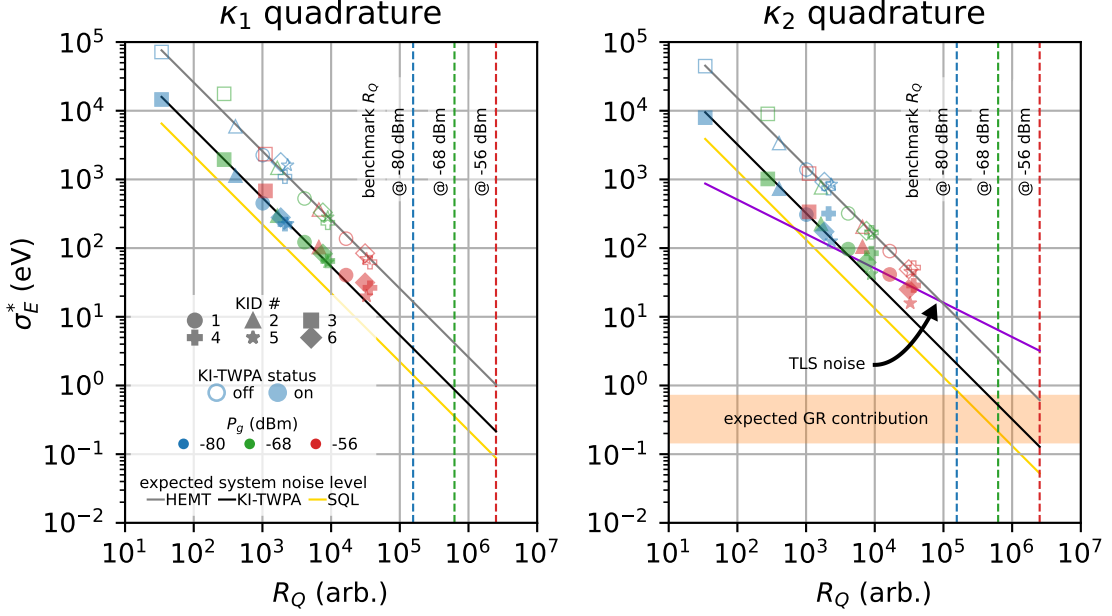


FIG. 4: Inferred energy resolution across orthogonal quadratures, resonator number, readout power, and operating configuration, plotted against the RF responsivity R_Q defined in Eq. 7, along with expected system noise levels for different scenarios. The vertical lines at different powers reflect benchmark R_Q quantities as discussed in text. In the κ_2 quadrature, the effect of TLS noise, expected to go as $P_g^{-1/4}$, is drawn suggestively in purple. Expected generation-recombination noise resolution limits (applicable to both quadratures, but shown only in κ_2) are illustrated by the shaded orange band.

as mentioned previously. Further study of β will require a dedicated energy source, such as a radioactive material or an LED, so as to improve statistics. For the purposes of this article, we assume the theoretical Mattis-Bardeen response to define the relative responsivity of the two quadratures.

An example of a timestream converted into quasiparticle units is shown for the κ_2 direction in Fig 3 Bottom Left and is the same pulse that is shown in Fig 3 Top Left. A single pole exponential was fit to this observed pulse and the time constant is displayed. The fit was then used to construct a signal template \tilde{s} , which in conjunction with a noise power spectral density J_{qp} was used to compute the optimally filtered resolution on quasiparticle density σ_{qp} as per the standard prescription found in Refs. [9, 25].

J_{qp} was computed for both $\kappa_{1,2}$ timestreams, and examples for MKID 5 are plotted in Fig. 3 Center and Right. The effect of the theoretically specified β on the relative noise level between quadratures is illustrated with the dashed arrow. The impact of the KI-TWPA on the readout noise is seen across all readout powers at the highest frequencies: around a decade-and-a-half of improvement, matching the $5\times$ system noise improvement from the spectrum analyzer measurement. At lower frequencies, both quadratures demonstrate significant noise coloring, progressively increasing with readout power. In the case of κ_2 , the resonator's intrinsic TLS noise dominates and exhibits a signature frequency dependence $f^{-1 \leq y \leq -0.5}$ below the roll-off frequency $\nu_r / (2Q_r)$ [26]. The exponent y is in general material and fabrication process dependent and given by the oscillatory behavior of the two-level system. TLS noise

of this form has been previously noted as limiting the noise performance of similarly designed MKIDs [9]. The κ_1 quadrature is not expected to exhibit TLS [26], and the noise follows a f^{-1} prescription at the highest readout power. One hypothesis for this noise is that it is sourced by long timescale transmission fluctuations. If correct, this noise may be removable in the future by the concurrent measurement of an off-resonance tone and subsequent subtraction of any correlated component between the on-resonance tone and the off-resonance tone. Similar techniques have been demonstrated for noise reduction in prior MKID measurements [8, 9].

\tilde{s} and J_{qp} were used to compute the optimally filtered quasiparticle resolution σ_{qp} , and the results are shown in Fig. 4. In order to project the ultimate energy threshold reach of a KIPM detector with KI-TWPA amplification, the results are converted to an inferred energy resolution σ_E^* of a hypothetical single resonator KIPM detector⁵, assuming the measured σ_{qp} for each MKID in the present array. We converted to σ_E^* with

$$\sigma_E^* = \frac{V_{sc}\Delta}{\eta_{ph}} \sigma_{qp}, \quad (6)$$

where $V_{sc} = 3 \times 10^4 \mu\text{m}^3$ is the superconducting absorber volume and η_{ph} is a phonon absorption to quasiparticle creation efficiency. We expect $\eta_{ph} = 0.3$ is achievable, from measurements in other phonon-mediated experimental designs [27].

⁵ In a multi-resonator KIPM detector, the energy resolution scales with $\sqrt{\#}$ of resonators.

The results of the inferred resolution calculation are shown in Fig. 4 for both the $\kappa_{1,2}$ directions, plotted against an *RF responsivity* quantity R_Q . This variable, first defined in Ref. [8], takes the form:

$$R_Q \equiv |V_r| \frac{Q_r^2}{|\hat{Q}_c|}, \quad (7)$$

where $|V_r|$ is the voltage amplitude of a nearby off-resonant tone *at the resonator*. Given the complexity and systematic uncertainties involved in extracting V_r in a real experiment, a relative measure of R_Q can be obtained by using V_{ADC} instead, which is measured at the DAQ in arbitrary ADC units. Conveniently, the diameter of a resonance circle in raw IQ space is $D = |V_{\text{ADC}}| Q_r / |\hat{Q}_c|$, which allowed for this relative R_Q to be computed as $D Q_r$. We note that $|V_{\text{ADC}}| \propto |a| \sqrt{P_g}$ and so depends on the readout power. Additionally, $R_Q \propto dS_{21}/dx|_{x=0}$ as computed from Eq. 4, emphasizing the role of R_Q as the RF responsivity.

Fig. 4 shows that R_Q dominates the energy performance of the investigated resonators due to the wide range of transmission and quality factors that were measured across the resonators. Two orders of magnitude may be gained in the energy resolution by rectifying R_Q of the resonator design to hit our displayed benchmark for all sensors. The design goal is a device transmission of unity and $Q_r \sim Q_c \sim 10^5$ so that $O(\mu\text{s})$ rise time information can be maintained, with ongoing efforts to improve R_Q using RF engineering techniques [28]. Higher readout powers are also beneficial but have the caveat of affecting detector linearity [29].

Fig. 4 also shows the inferred energy resolution improvement from KI-TWPA operation as the level shift between the KI-TWPA on and off points. For the KI-TWPA off points, R_Q as measured at the DAQ was multiplied by G_{pa} to put it on the same footing as the KI-TWPA on scenario. This step ensured the $R_Q \propto |V_r|$ scaling. The resolution improvement is also recorded as the scatter points in Fig. 2 Top. The expected system noise levels are illustrated via the solid lines that pass through the points: the HEMT-dominated system noise level is determined from a fit to the points with the KI-TWPA off, and the expected system noise levels of the KI-TWPA-dominated and the SQL cases come from the spectrum analyzer analysis.

At the lowest readout powers and for resonators of low R_Q , the full range of expected improvement is observed. At higher readout powers, two stories emerge: 1) in the κ_1 quadrature, the aforementioned f^{-1} noise begins to contribute more; 2) in the κ_2 quadrature, TLS noise begins to dominate the noise performance. TLS noise is expected to go as $P_g^{-1/4}$, and the points at higher readout powers in Fig. 4 Right follow this relation. It is believed that this particular KIPM detector exhibits elevated TLS noise due to the presence of multiple oxide-forming films during the fabrication process. Crucially then, the resolution improvement due to parametric amplification is dampened by these effects that will have to be solved to realize a quantum-limited sensor at higher readout powers. Furthermore, the ultimate achievable resolution performance of SQL amplification is still a factor of $\sqrt{\langle N_{\text{sys}} \rangle} \sim 3$ below current performance, limited by the prior discussed passive component systematics

and KI-TWPA gain.

One unobserved noise source in this analysis that will be important going forward is generation-recombination (GR) noise of the quiescent quasiparticle population (density n_0). The observed lifetime from Fig. 3 Bottom Left implies $n_0 \approx 475 \mu\text{m}^{-3}$ [21]. Using the current design V_{sc} and assuming Poisson fluctuations about the total quasiparticle number, GR noise will contribute $\sigma_{E,\text{GR}}^* = 0.7$ eV toward the inferred energy resolution. Thus, improvements to the resolution past this point will require upper limits on the total quasiparticle number or, equivalently, lower limits on the quasiparticle lifetime. Relatedly, a density of $n_0 = 25 \mu\text{m}^{-3}$ has been shown in the MKID literature [30] (equivalent to $\sigma_{E,\text{GR}}^* = 0.15$ eV). This range of GR noise-dominated resolution is included in Fig. 4. Further ideas to decrease n_0 focus on mitigating the effects of blackbody pair-breaking radiation [20, 31]. Increasing the quasiparticle lifetime has the added benefit of narrowing the bandwidth of \tilde{s} , improving the resolution by $1/\sqrt{\tau_{\text{qp}}}$ [25].

V. APPLICATION TO A RARE-EVENT SEARCH AND CONCLUSION

To explore the ramifications of a meV resolving KIPM detector, consider the case of searching for a light dark matter particle (χ) via its elastic scattering on a heavier target (e.g. a silicon nucleus, M). The maximum energy transfer in such a two-body collision, if $m_M \gg m_\chi$, is $E_{\text{max}} \approx 2m_\chi^2 v_\chi^2 / m_M$, where v_χ is the particle velocity (capped at ~ 600 km/s for dark matter due to Milky Way constraints). With an experimental threshold of $5\sigma_E$, a silicon target KIPM detector benefiting from SQL amplification with $\sigma_E \approx 200$ meV would be sensitive to a dark matter mass of $m_\chi \approx 55$ MeV. Current state-of-the-art experiments probe dark matter masses of $m_\chi \sim 100$ MeV [32, 33], which suggests significant expansion into previously unexplored dark matter coupling parameter space.

In summary, we have demonstrated the effect of low noise amplifications on KIPM detector readout. We ascertain that significant improvements to the substrate energy resolution on the order of $5\times$ can be achieved by pairing these devices with KI-TWPA parametric amplifiers. The limiting case of system noise N_{sys} close to 1 can in part be achieved with better passive components and better RF engineering, making KI-TWPAs an ideal addition to next generation rare-event search experiments. However, resonator and quasiparticle physics, like the presence of two-level systems, can impact sensitivity and further work is required to overcome these limitations.

ACKNOWLEDGMENTS

We thank N. Klimovich for assistance in understanding KI-TWPA behavior. We thank SLAC and FNAL collaborators for insightful conversations regarding MKIDs and parametric amplification. The research was carried out at the Jet Propulsion Laboratory, California Institute of Technology, under a contract with the National Aeronautics and Space Administration (80NM0018D0004). K.R. is supported in part by National Sci-

ence Foundation PHY Grant 2209581. O.W. is supported by NASA NSTGRO Award 80NSSC20K1223. We also acknowl-

edge support from the Department of Energy, DESC0011925F Fermilab, LDRD Subcontract 672112.

-
- [1] P. K. Day, H. G. LeDuc, B. A. Mazin, A. Vayonakis, and J. Zmuidzinas, *Nature* **425**, 817 (2003).
- [2] G. Hammer, S. Wuensch, K. Ilin, and M. Siegel, in *Journal of Physics: Conference Series*, Vol. 97 (IOP Publishing, 2008) p. 012044.
- [3] S. Shu, M. Calvo, J. Goupy, S. Leclercq, A. Catalano, A. Bideaud, A. Monfardini, and E. F. Driessen, *Applied Physics Letters* **113** (2018).
- [4] G. Ulbricht, B. A. Mazin, P. Szypryt, A. B. Walter, C. Bockstiegel, and B. Bumble, *Applied Physics Letters* **106** (2015); R. Adam, A. Adane, P. Ade, P. André, A. Andrianasolo, H. Aussel, A. Beelen, A. Benoit, A. Bideaud, N. Billot, *et al.*, *Astronomy & Astrophysics* **609**, A115 (2018); S. R. Golwala, C. Bockstiegel, S. Brugger, N. G. Czakon, P. K. Day, T. P. Downes, R. Duan, J. Gao, A. K. Gill, J. Glenn, *et al.*, in *Millimeter, Submillimeter, and Far-Infrared Detectors and Instrumentation for Astronomy VI*, Vol. 8452 (SPIE, 2012) pp. 33–53; S. R. Meeker, B. A. Mazin, A. B. Walter, P. Strader, N. Fruitwala, C. Bockstiegel, P. Szypryt, G. Ulbricht, G. Coiffard, B. Bumble, *et al.*, *Publications of the Astronomical Society of the Pacific* **130**, 065001 (2018).
- [5] S. Doyle, P. Mauskopf, J. Naylon, A. Porch, and C. Duncombe, *Journal of Low Temperature Physics* **151**, 530 (2008).
- [6] D. Moore, S. Golwala, B. Bumble, B. Cornell, P. Day, H. LeDuc, and J. Zmuidzinas, *Applied Physics Letters* **100** (2012).
- [7] L. Cardani, N. Casali, I. Colantoni, A. Cruciani, S. Di Domizio, M. Martinez, V. Pettinacci, G. Pettinari, and M. Vignati, *The European Physical Journal C* **81**, 636 (2021).
- [8] K. Ramanathan, T. Aralis, R. Basu Thakur, B. Bumble, Y.-Y. Chang, O. Wen, and S. R. Golwala, *Journal of Low Temperature Physics* **209**, 457 (2022).
- [9] O. Wen, T. Aralis, R. Basu Thakur, B. Bumble, Y.-Y. Chang, K. Ramanathan, and S. Golwala, *Journal of Low Temperature Physics* **209**, 510 (2022).
- [10] J. Zmuidzinas, *Annu. Rev. Condens. Matter Phys.* **3**, 169 (2012).
- [11] O. Noroozian, J. Gao, J. Zmuidzinas, H. G. LeDuc, and B. A. Mazin, in *AIP Conference Proceedings*, Vol. 1185 (American Institute of Physics, 2009) pp. 148–151.
- [12] H. Nyquist, *Physical review* **32**, 110 (1928).
- [13] C. M. Caves, *Physical Review D* **26**, 1817 (1982).
- [14] C. M. Caves, *Physical Review D* **23**, 1693 (1981).
- [15] M. Esposito, A. Ranadive, L. Planat, S. Leger, D. Fraudet, V. Jouanny, O. Buisson, W. Guichard, C. Naud, J. Aumentado, *et al.*, *Physical Review Letters* **128**, 153603 (2022).
- [16] J. Aumentado, *IEEE Microwave magazine* **21**, 45 (2020).
- [17] B. Ho Eom, P. K. Day, H. G. LeDuc, and J. Zmuidzinas, *Nature Physics* **8**, 623 (2012).
- [18] N. S. Klimovich, *Traveling Wave Parametric Amplifiers and Other Nonlinear Kinetic Inductance Devices*, *Ph.D. thesis*, California Institute of Technology (2022); N. Klimovich, P. Day, S. Shu, B. H. Eom, J. Leduc, and A. Beyer, arXiv preprint arXiv:2306.11028 (2023).
- [19] N. Zobrist, B. H. Eom, P. Day, B. A. Mazin, S. R. Meeker, B. Bumble, H. G. LeDuc, G. Coiffard, P. Szypryt, N. Fruitwala, *et al.*, *Applied Physics Letters* **115** (2019).
- [20] Y.-Y. Chang, *SuperCDMS HVeV Run 2 Low-Mass Dark Matter Search, Highly Multiplexed Phonon-Mediated Particle Detector with Kinetic Inductance Detector, and the Blackbody Radiation in Cryogenic Experiments*, *Ph.D. thesis*, California Institute of Technology (2023).
- [21] S. B. Kaplan, C. C. Chi, D. N. Langenberg, J. J. Chang, S. Jafarey, and D. J. Scalapino, *Phys. Rev. B* **14**, 4854 (1976).
- [22] *ZDSS-5G6G-S+ Suspended Substrate Diplexer*, *Minicircuits* (2022), rev. B; *K250 Bias Tee*, Anritsu (2021), rev. D; C. Diez and J. D. Gallego, *CRYOGENIC MEASUREMENTS ISOLATORS CTH1365K10 A151 SN 106, 107, 108, 109, 110*, Tech. Rep. Yebes/FPSS/TN/2003-003 (Centro Astronómico de Yebes, 2003).
- [23] M. S. Khalil, M. Stoutimore, F. Wellstood, and K. Osborn, *Journal of Applied Physics* **111** (2012).
- [24] D. C. Mattis and J. Bardeen, *Physical Review* **111**, 412 (1958).
- [25] S. R. Golwala, *Exclusion limits on the WIMP-nucleon elastic-scattering cross-section from the Cryogenic Dark Matter Search* (University of California, Berkeley, 2000).
- [26] J. Gao, *The physics of superconducting microwave resonators* (California Institute of Technology, 2008).
- [27] R. Ren, C. Bathurst, Y. Chang, R. Chen, C. Fink, Z. Hong, N. Kurinsky, N. Mast, N. Mishra, V. Novati, *et al.*, *Physical Review D* **104**, 032010 (2021); M. Pyle, B. Serfass, P. Brink, B. Cabrera, M. Cherry, N. Mirabolfathi, L. Novak, B. Sadoulet, D. Seitz, K. Sundqvist, *et al.*, in *AIP Conference Proceedings*, Vol. 1185 (American Institute of Physics, 2009) pp. 223–226.
- [28] H. Kim and R. Franklin-Drayton, *IEEE transactions on microwave theory and techniques* **57**, 442 (2009).
- [29] S. R. Siegel, *A Multiwavelength Study of the Intracluster Medium and the Characterization of the Multiwavelength Sub/millimeter Inductance Camera* (California Institute of Technology, 2016).
- [30] P. De Visser, J. Baselmans, P. Diener, S. Yates, A. Endo, and T. Klapwijk, *Physical review letters* **106**, 167004 (2011).
- [31] P. J. de Visser, J. Baselmans, J. Bueno, N. Llombart, and T. Klapwijk, *Nature communications* **5**, 3130 (2014).
- [32] G. Angloher, S. Banik, G. Benato, A. Bento, A. Bertolini, R. Breier, C. Bucci, J. Burkhart, L. Canonica, A. D’Addabbo, *et al.*, *Physical Review D* **107**, 122003 (2023).
- [33] J. Collar, *Physical Review D* **98**, 023005 (2018).